Electron density and conductance variationsin the auroral ionosphere during substorms; influence of solar wind and plasma sheet state.

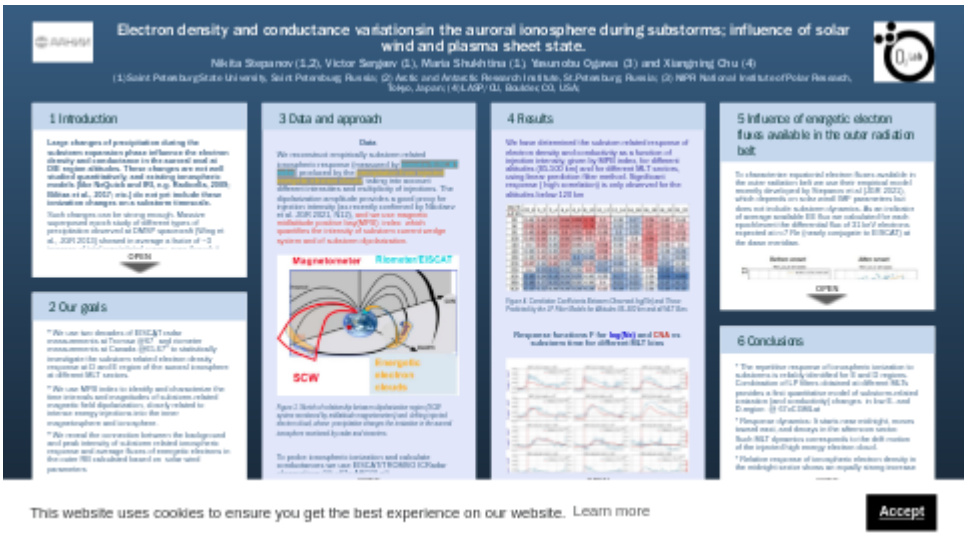

Nikita Stepanov (1,2), Victor Sergeev (1), Maria Shukhtina (1), Yasunobu Ogawa (3) and Xiangning Chu (4)

(1) Saint Petersburg State University, Saint Petersburg, Russia; (2) Arctic and Antarctic Research Institute, St.Petersburg, Russia; (3) NIPR National Institute of Polar Research, Tokyo, Japan; (4) LASP/CU, Boulder, CO, USA;

PRESENTED AT:

1 INTRODUCTION

Large changes of precipitation during the substorm expansion phase influence the electron density and conductance in the auroral oval at D/E region altitudes. These changes are not well studied quantitatively, and existing ionospheric models (like NeQuick and IRI, e.g. Radicella, 2009; Bilitza et al., 2017; etc.) do not yet include these ionization changes on a substorm timescale.

Such changes can be strong enough. Massive superposed epoch study of different types of precipitation observed at DMSP spacecraft (Wing et al., JGR 2013) showed in average a factor of ~3 increase of total precipitated power, even though it did not include energetic particles above 30keV and provided averaging over substorms of different intensities (with dominant contribution of modest events). Measurements of electron density altitudinal profiles made by Incoherent Scatter Radars provided excellent illustrations of sudden and large electron density changes during substorms (up to a few orders of magnitude in E- and D-regions , e.g., Partamies et al., 2011), with fast and large local conductivity enhancements, associated with strong variations of auroral zone currents (Davies & Lester, 1999; Hosokawa & Ogawa, 2010; Kirkwood et al., 1988; Sugino et al., 2002). Important for Space Weather and specific for substorms are the strong D-region perturbations in the morning auroral zone, associated with hard electron precipitation (e.g., Hosokawa & Ogawa, 2010, 2015; Miyoshi et al., 2015; Oyama et al., 2017). All these perturbations manifest a strong variability and complicated azimuthal evolution (e.g. Berkey et al.1974, Beharrell et al., 2015). Despite all efforts, the overall picture of substorm-related ionospheric variations is still highly fragmentary and incomplete. **Quantitative characterization of substorm-related ionization changes at different altitudes and local time sectors in the ionosphere**, which takes into account a wide range of substorm intensities and multiplicity of activations, **constitutes the main objective of our study.**

Although there exist several different ways of accelerating and precipitating electrons during substorms (incl. current sheet acceleration, field-aligned acceleration, WP interactions, etc) consideration of substorm injections offers a particularly perspective route for organizing the substorm effects in space and time. Enhanced earthward plasma flows bring accelerated particles and magnetic flux into the nightside inner magnetosphere, producing the magnetic field dipolarization and injecting energetic plasma (e.g., Li et al 1998, Yang et al.2011, Gabrielse et al.2018). Drifting around the Earth, the energetic plasma precipitates into the ionosphere. Energetic electron precipitations (EEP, tens keV) produce ionization in the D/E-regions. Close relationship between dipolarizations and injections allows the use of the dipolarization amplitude as a proxy for injection intensity (as recently confirmed by Nikolaev et al. JGR 2021, N12). Recently Sergeev et al. (2020) demonstrated the efficiency of linear prediction filter method to organize the substorm effects in space and time based on magnetic MPB index as a proxy of dipolarization amplitudes. In a similar way, **here we reconstruct empirical response functions to reveal spatial/temporal changes of ionization at different altitudes during substorms.**

Whereas localized sporadic plasma injections from the tail plasma sheet can be a core process, the amount of energetic electron flux available in the outer radiation belt prior to injection can be another important factor controlling the level of energetic electron precipitation during substorms. Here we show initial results demonstrating the importance of this factor for the D-region ionization.

2 OUR GOALS

* We use two decades of EISCAT radar measurements at Tromsø @67^{o} and riometer measurements at Canada @65-67^{o} to statistically investigate the substorm related electron density response at D and E region of the auroral ionosphere at different MLT sectors.

* We use MPB index to identify and characterize the time intervals and magnitudes of substorm-related magnetic field dipolarization, closely related to intense energy injections into the inner magnetosphere and ionosphere.

* We reveal the connection between the background and peak intensity of substorm related ionospheric response and average fluxes of energetic electrons in the outer RB calculated based on solar wind parameters

3 DATA AND APPROACH

Data

We reconstruct empirically substorm related ionospheric response (measured by riometer/EISCAT radar) produced by the precipitation from injected energetic electron clouds, taking into account different intensities and multiplicity of injections. The dipolarization amplitude provides a good proxy for injection intensity (as recently confirmed by Nikolaev et al. JGR 2021, N12), and we use magnetic midlatitude positive bay(MPB) index which quantifies the intensity of substorm current wedge system and of substorm dipolarization.

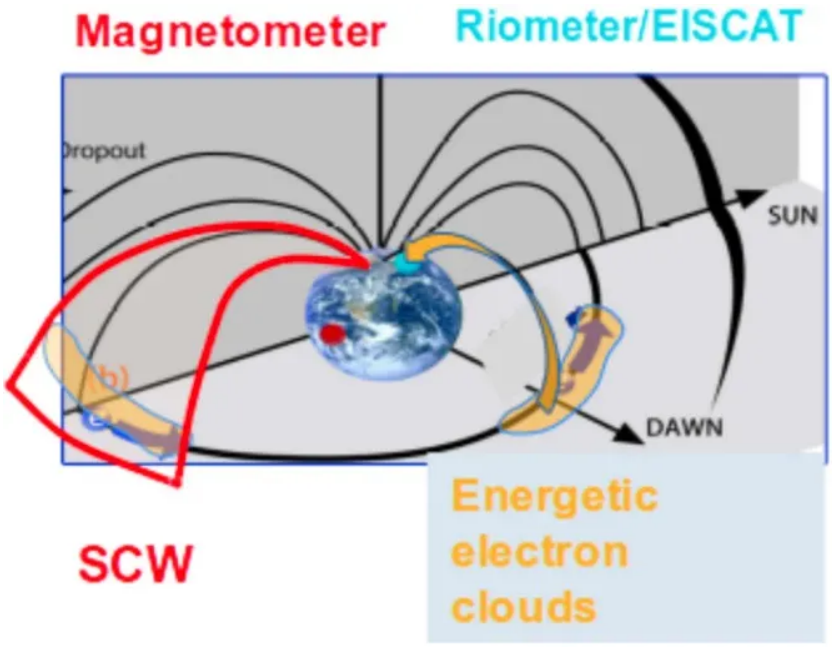

Figure 1. Sketch of relationship between dipolarization region (SCW system monitored by midlatitude magnetometers) and drifting injected electron cloud, whose precipitation changes the ionization in the auroral ionosphere monitored by radar and riometers.

To probe ionospheric ionization and calculate conductances we use EISCAT/TROMSO ICRadar observations (@ ~67o AACGLat)

- 1996 - 2018, averaged to 5m resolution
- CP1, CP2, CP6, arc1 and beata modes
- log(Ne), conductances Σh, Σp,
- H = 85-120 km (in this analyses)

For the independent control of ionization response to injections we also use CNA (cosmic noise absorption) data from 5 Canadian riometers (also @ ~67o AACGLat)

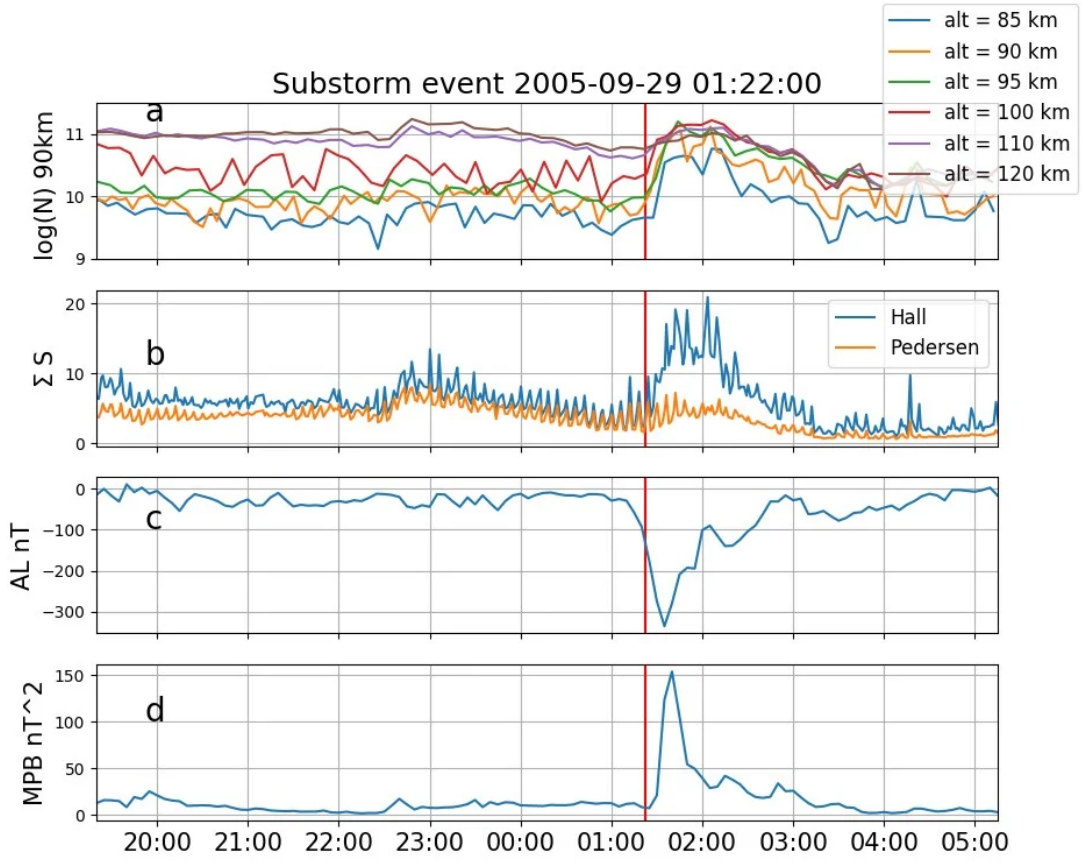

Fig 2. Example of substorm event in ~03–05 h MLT sector: (a) e-density at altitudes between 85 and 120 km; (b) ionospheric conductances (ignore periodic changes in the electrical conductance which are due to the periodic swinging of the antenna direction); (c) AL index; (d) MPB index variations. Substorm started at 01:22 UT

To select the substorm intervals and as proxy of dipolarization /injection magnitude, we use the MPB index (McPherron and Chu, Sp.Sci.Rev.,2017) which characterizes nightside midlatitude magnetic variations caused by the substorm current wedge. Altogether we selected ~480 near-isolated substorms for response function analyses in 1996-2015. Based on 5 min MPB averages, we use positive values of MPB increments at 5 min time step ($T_i = MPB_{i+1}^{1/2} - MPB_i^{1/2}$) as formal proxies of dipolarizations (see Figure 3 for an example of preparing the matrix T). In the linear prediction filter (LPF) method the response of the output quantity Ai (electron density, or conductance, etc at time step i) is determined as a sum of contributions from input quantities Tj (dipolarization proxies) acting at time steps j=i+k (k varied between -m and N) , i.e. $A_i = \sum_{k=1}^{N} F_k T_{i-N+k} + A_0$. In our case (with a 5min time step, N=48 and m=12) we take into account the actions from events that occurred between [T0-4hrs; T0+1hr]. By solving the linear matrix equation we get the linear prediction filter Fk , the desired response function to the unit-scale injection. The method is useful in case of distributed (in time) or multiple actions of different intensities, as typical for substorms. in form

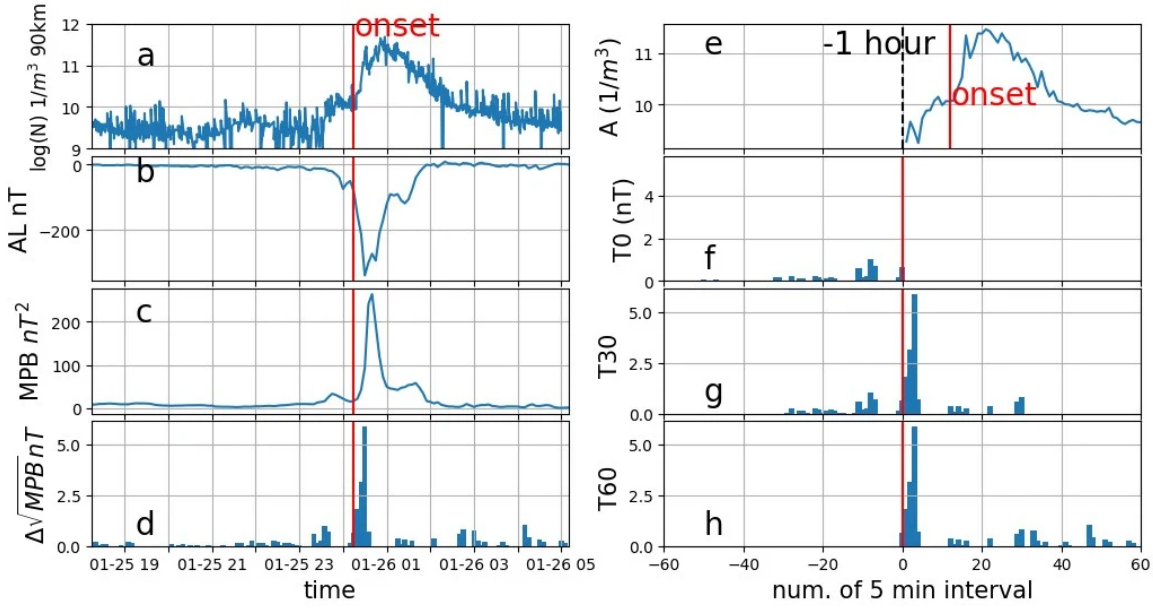

Figure 3. Example of contributions to vector A and matrix T from substorm starting at 2009-01-26 00:15 UTC. (a) logarithm of electron density at 90 km; (b) AL index; (c) MPB index; (d) dipolarization proxies- increments of square root of MPB index MPB1/2(t + 5 min) - MPB1/2(t); (e) vector A; (f, g, and h) prepared for first, 30th and 60th rows of matrix T.

4 RESULTS

We have determined the substom related response of electron density and conductivity as a function of injection intensity, given by MPB index, for different altitudes (85-500 km) and for different MLT sectors, using linear prediction filter method. Significant response (high correlation) is only observed for the altitudes below 120 km

MLT h / Alt km	22_0	0_2	2_4	4_6	6_8	8_10	10_12	12_14	14_16	16_18	18_20	20_22
85	0.41	0.49	0.52	0.64	0.69	0.74	0.5	0.36	0.27	0.54	0.47	0.41
90	0.51	0.54	0.52	0.63	0.62	0.74	0.51	0.32	0.29	0.57	0.53	0.5
95	0.46	0.56	0.46	0.6	0.55	0.6	0.49	0.3	0.29	0.6	0.52	0.51
100	0.43	0.54	0.37	0.56	0.49	0.5	0.5	0.32	0.4	0.64	0.51	0.49
110	0.4	0.51	0.35	0.57	0.45	0.41	0.54	0.36	0.46	0.6	0.42	0.4
120	0.36	0.43	0.35	0.52	0.36	0.34	0.54	0.39	0.47	0.57	0.34	0.29
150	0.38	0.45	0.46	0.51	0.2	0.26	0.49	0.32	0.41	0.6	0.3	0.29
200	0.47	0.34	0.49	0.33	0.25	0.45	0.27	0.26	0.36	0.52	0.27	0.36
250	0.4	0.23	0.21	0.28	0.35	0.5	0.22	0.31	0.32	0.4	0.15	0.25
300	0.16	0.24	0.18	0.24	0.25	0.36	0.35	0.17	0.25	0.38	0.09	0.09
350	0.18	0.27	0.22	0.24	0.32	0.38	0.4	0.21	0.22	0.38	0.17	0.17
500	0.17	0.22	0.26	0.24	0.24	0.24	0.42	0.18	0.23	0.34	0.15	0.15

Figure 4. Correlation Coefficients Between Observed log(Ne) and Those Predicted by the LP Filter Models for Altitudes 85–500 km and all MLT Bins

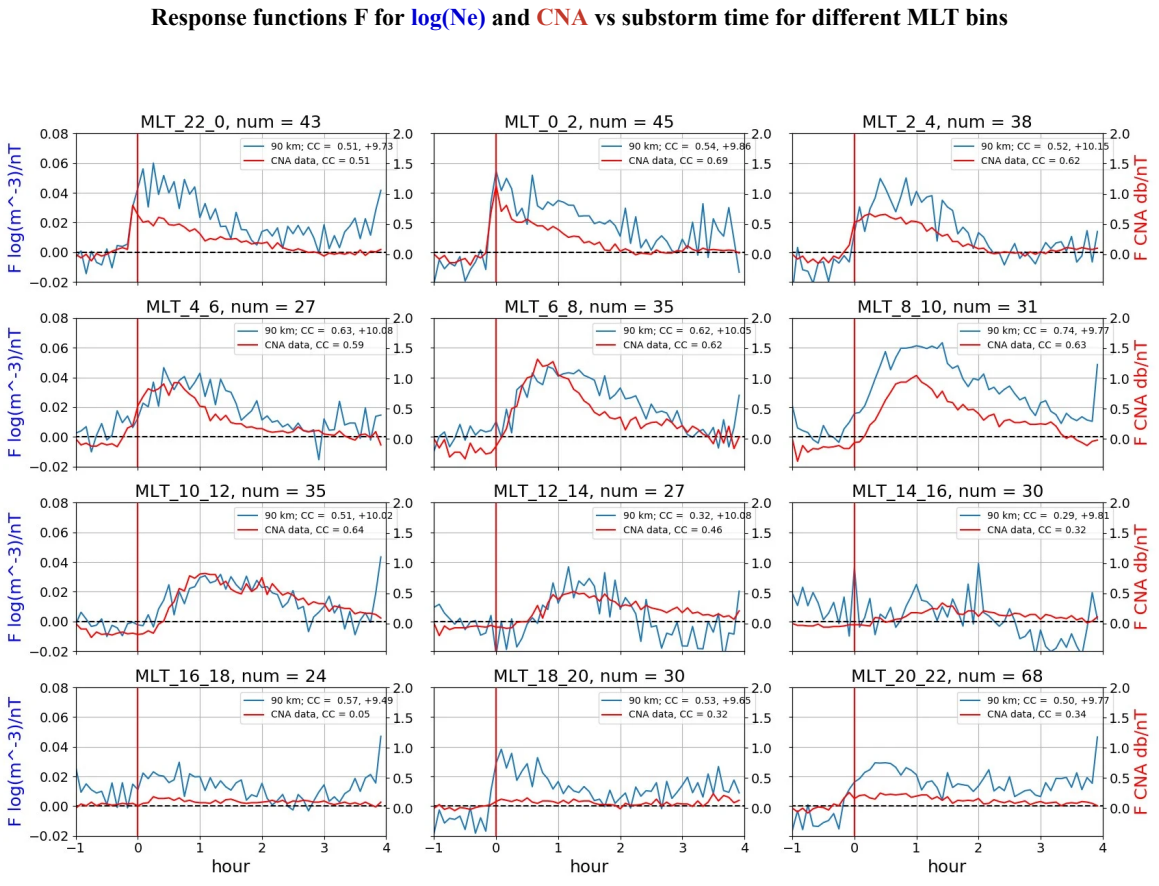

Figure 5. Blue lines - the response functions for electron density at h = 90 km against substorm time, different panels correspond to different MLT sectors. Red line - the response functions for cosmic noise absorption (Sergeev et al., 2020). The red vertical line shows the substorm onset. Corresponding Pearson correlation coefficient and A0 values (see 3) are shown in the top right corner of each panel.

- MLT variation of ionospheric response F at 90 km
  - Immediate response at the midnight
  - delayed response in the morning sector
  - decaying at the noon sector

- Comparison to CNA response function shows similar shapes and MLT changes of ionospheric response (except evening); similar results from different data/period/event sets confirm the robustness of the inferred ionospheric response.
- CC ~0.6 near midnight, ~0.4 near noon

Response functions for log(Ne) at different altitudes

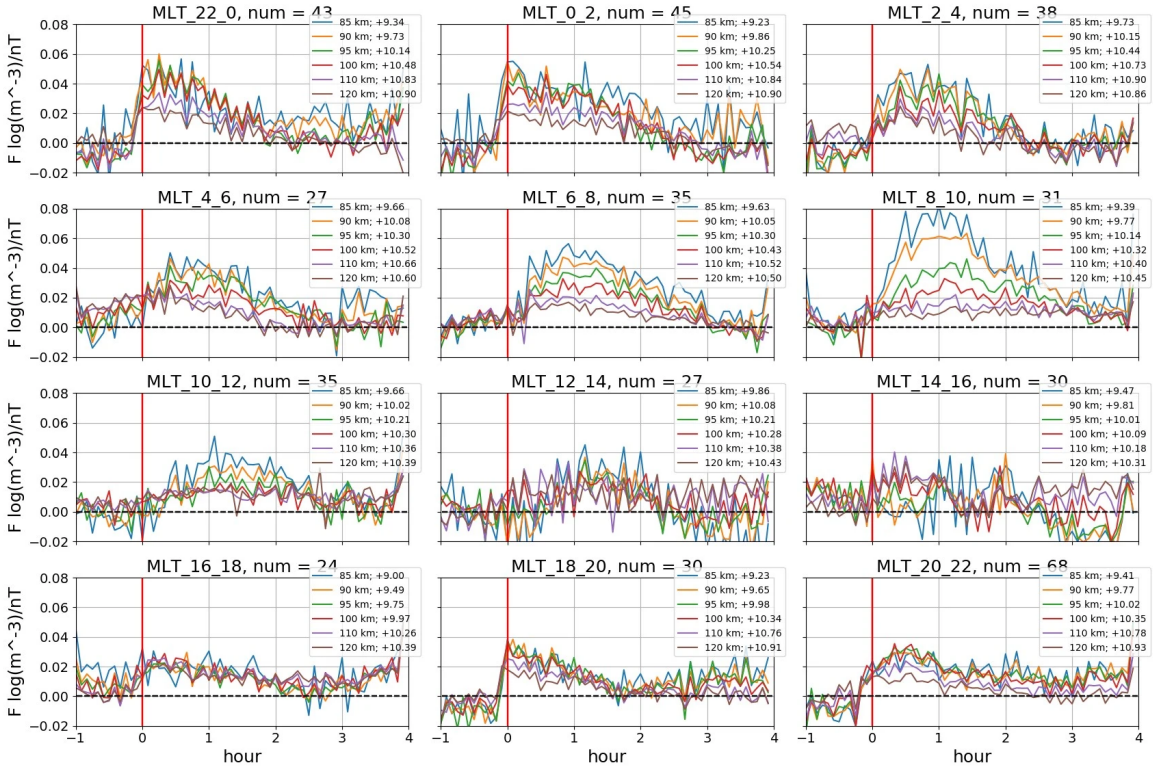

Figure 6. Color-coded response functions of electron density for altitudes between 85 and 120 km in different MLT sectors. The red vertical line shows the substorm onset. The corresponding baseline values A0 are given in the legends for each altitude

- Response functions at different altitudes and MLTs are individual (different A0 and amplitude)
- Weaker relative response for higher altitude
- Maximum relative increase is observed
  - at 85-100 km in the midnight sector
  - at morning dominate at 85 km

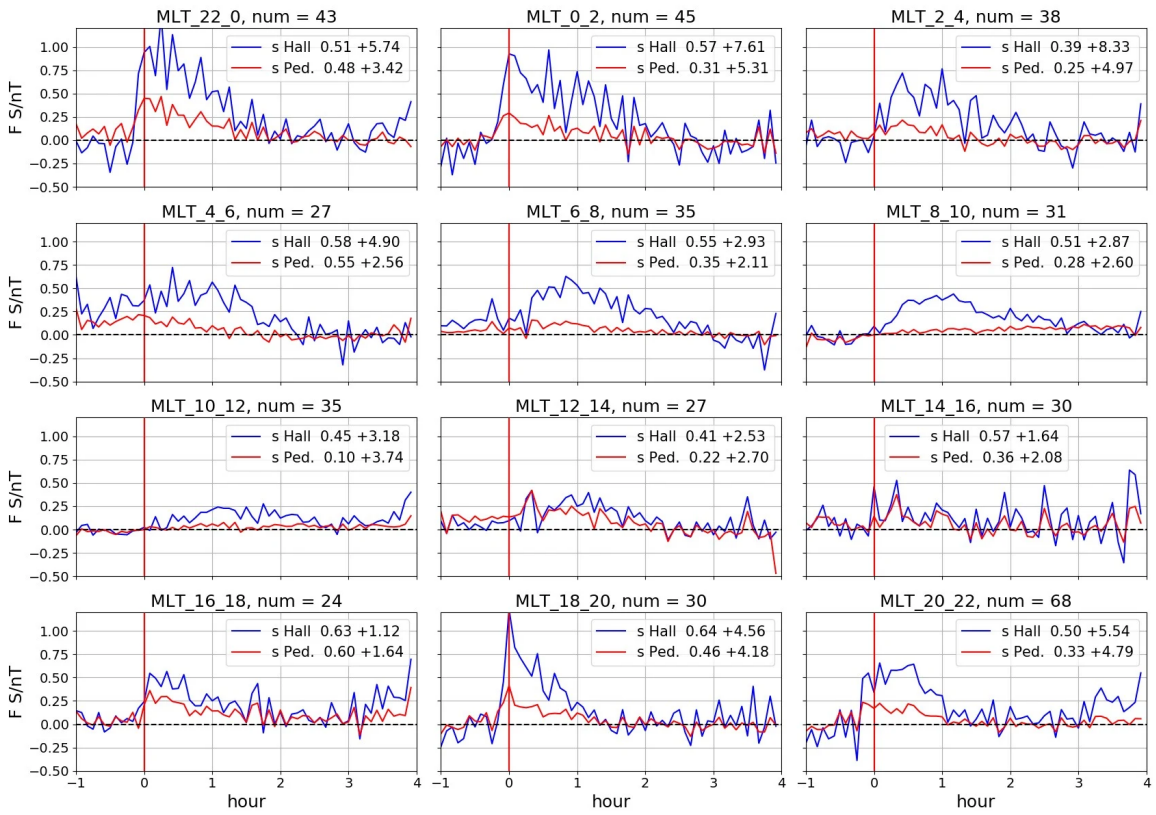

Figure 7. The response functions for integral Hall and Pedersen conductances in different MLT sectors. Red vertical line shows the substorm onset. Corresponding correlation coefficient and A0 are given in the top right corner

- Substorm response is systematically larger for Σh than for Σp
- Similar MLT variations of Σh and Ne at 100 km in midnight-morning sector (except evening)
- Weaker response of Σh and Σp in the morning sector due to dumped response in the E-region ionization.

5 INFLUENCE OF ENERGETIC ELECTRON FLUXES AVAILABLE IN THE OUTER RADIATION BELT

To characterize equatorial electron fluxes available in the outer radiation belt we use their empirical model recently developed by Stepanov et al (JGR 2021), which depends on solar wind/ IMF parameters but does not include substorm dynamics. As an indicator of average available EE flux we calculated for each epoch/event the differential flux of 31 keV electrons expected at r=7 Re (nearly conjugate to EISCAT) at the dawn meridian.

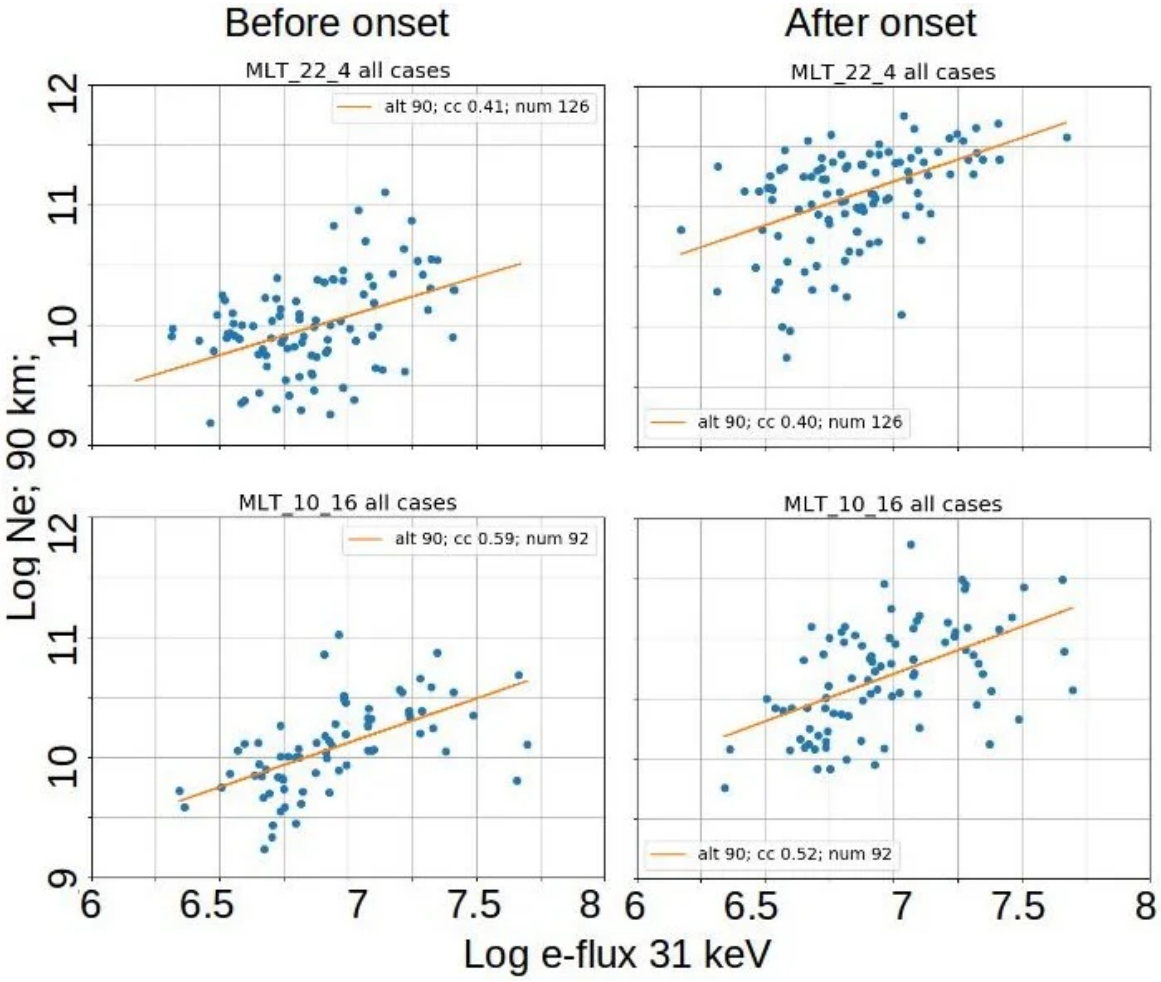

Figure 8. Relationship between model-based equatorial electron fluxes at 7 Re, 270o SM and ionospheric electron density at 90 km before substorm onset and maximum value during substorm

There exists an obvious correlation between average available equatorial electron fluxes and ionization values at h=90km, for both presubstorm and peak substorm situations, which needs further investigation.

6 CONCLUSIONS

* The repetitive response of ionospheric ionization to substorms is reliably identified for E and D regions. Combination of LP filters obtained at different MLTs provides a first quantitative model of substorm-related ionization (and conductivity) changes in low E- and D-region @ 67oCGMLat

* Response dynamics: It starts near midnight, moves toward east, and decays in the afternoon sector. Such MLT dynamics corresponds to the drift motion of the injected high energy electron cloud.

* Relative response of ionospheric electron density in the midnight sector shows an equally strong increase at 85-100 km, but in the morning sector the relative response dominates at 85-90 km. Such altitudinal distribution results in stronger enhancements of integral Hall (and Pedersen) conductances in the midnight sector than in the morning sector.

* Average e-flux available in the outer radiation belt affects background D-region ionization as well as its peak values produced during substorms.

ABSTRACT

Enhanced precipitation of magnetospheric energetic particles during substorms increases ionospheric electron density and conductance. Such enhancements, which have timescales of a few hours, are not reproduced by the current ionospheric models. Using EISCAT (Tromso) measurements we reconstruct the substorm related response of electron densities and conductances in the ionosphere with respect to the intensity of substorm injections. We also investigate how the intensity of the response is influenced by the variations of the plasma sheet high energy (tens keV) fluxes and solar wind state. To characterise the intensity of substorm injection at a 5min time step we use the midlatitude positive bay (MPB) index which basically responds to the substorm current wedge variations. We build response functions (LPF filters) between T0-1h and T0+4hrs (T0 is a substorm onset time) in different MLT sectors to estimate the magnitude and delays of the ionospheric density response at different altitudes. The systematic and largest relative substorm related changes are mostly observed in the lowest part of E and in D regions. It starts and reaches maximum magnitude near midnight, from which it mainly propagates toward east, where it decays when passing into the noon-evening sector. Such MLT structure corresponds to the drift motion of the injected high energy electron cloud in the magnetosphere. Besides the injection intensity, we look at how the magnitude of the response depends on the energetic (tens keV) fluxes level in the plasma sheet before the substorm onset. We use a previously developed empirical model of the plasma sheet fluxes with solar wind parameters as inputs to count the plasma sheet fluxes with energy 10, 31 and 93 keV in the reference point of transition region (6 Re, 270o SM Long). We found that during enhanced high energy fluxes in the plasma sheet before the substorm (fast solar wind, high solar wind reconnection electric field) the background ionisation in the ionosphere, as well as the peak ionisation value during the substorm, are higher. This implies that together with substorm intensity the prehistory of the plasma sheet/solar wind state forms the magnitude development of substorm related ionospheric response. Research was supported by Russian Ministry of Science and Higher Education grant № 075-15-2021-583

REFERENCES

Berkey, F. T., Driatskiy, V. M., Henriksen, K., Hultqvist, B., Jelly, D. H., Shchuka, T. I., et al. (1974). A synoptic investigation of particle precipitation dynamics for 60 substorms in IQSY (1964–1965) and IASY (1969). Planetary and Space Science, 22(2), 255–307. https://doi.org/10.1016/0032-0633(74)90028-2

Beharrell, M. J., Honary, F., Rodger, C. J., & Clilverd, M. A. (2015). Substorm-induced energetic electron precipitation: Morphology and prediction. Journal of Geophysical Research: Space Physics, 120, 2993–3008. https://doi.org/10.1002/2014JA020632

Davies, J., & Lester, M. (1999). The relationship between electric fields, conductances and currents in the high-latitude ionosphere: Astatistical study using eiscat data. Annales Geophysicae, 17, 43–52. https://doi.org/10.1007/s00585-999-0043-3

Davies, J., & Lester, M. (1999). The relationship between electric fields, conductances and currents in the high-latitude ionosphere: A statistical study using eiscat data. Annales Geophysicae, 17, 43–52. https://doi.org/10.1007/s00585-999-0043-3

Hosokawa, K., & Ogawa, Y. (2010). Pedersen current carried by electrons in auroral D-region. Geophysical Research Letters, 37(18), L18103. https://doi.org/10.1029/JA086iA04p02295

Hosokawa, K., & Ogawa, Y. (2015). Ionospheric variation during pulsating aurora. Journal of Geophysical Research: Space Physics, 120, 5943–5957. https://doi.org/10.1002/2015JA021401

Kirkwood, S., Opgenoorth, H., & Murphree, J. S. (1988). Ionospheric conductivities, electric fields and currents associated with auroral substorms measured by the EISCAT radar. Planetary and Space Science, 36(12), 1359–1380. https://doi.org/10.1016/0032-0633(88)90005-0

Miyoshi, Y., Oyama, S., Saito, S., Kurita, S., Fujiwara, H., Kataoka, R., et al. (2015). Energetic electron precipitation associated with pulsating aurora: EISCAT and Van Allen Probe observations. Journal of Geophysical Research: Space Physics, 120, 2754–2766. https://doi.org/10.1002/2014JA020690

McPherron, R. L., & Chu, X. (2017). The mid-latitude positive bay and the MPB index of substorm activity. Space Science Reviews, 206,91–122. https://doi.org/10.1007/s11214-016-0316-6

A. V. Nikolaev, V. A. Sergeev, M. A. Shukhtina, E. Spanswick, D. D. Rogov, and N. A. Stepanov (2021). Study of Substorm-Related Auroral Absorption: Latitudinal Width and Factors Affecting the Peak Intensity of Energetic Electron Precipitation; Journal of Geophysical Research: Space Physics. DOI: 10.1029/2021JA029779

Oyama, S., Kero, A., Rodger, C. J., Clilverd, M. A., Miyoshi, Y., Partamies, N., et al. (2017). Energetic electron precipitation and auroral morphology at the substorm recovery phase. Journal of Geophysical Research: Space Physics, 122, 6508–6527.https://doi.org/10.1002/2016JA023484

Partamies, N., Juusola, L., Tanskanen, E., Kauristie, K., Weygand, J. M., & Ogawa, Y. (2011). Substorms during different storm phases. Annales Geophysicae, 29, 2031–2043. https://doi.org/10.5194/angeo-29-2031-2011

Sergeev, V. A., Shukhtina, M. A., Stepanov, N. A., Rogov, D. D., Nikolaev, A. V., Spanswick, E., et al. (2020). Toward the reconstruction of substorm-related dynamical pattern of the radio wave auroral absorption. Space Weather, 18, e2019SW002385. https://doi.org/10.1029/2019SW002385

Stepanov, N. A., Sergeev, V. A., Sormakov, D. A., Andreeva, V. A., Dubyagin, S. V., Ganushkina, N., et al. (2021). Superthermal proton and electron fluxes in the plasma sheet transition region and their dependence on solar wind parameters. Journal of Geophysical Research: Space Physics, 126, e2020JA028580. https://doi.org/10.1029/2020JA028580

Sugino, M., Fujii, R., Nozawa, S., Buchert, S., Opgenoorth, H., & Brekke, A. (2002). Relativecontribution of ionospheric conductivity and electric field to ionospheric current. Journal of Geophysical Research, 107(A10), 1330. https://doi.org/10.1029/2001ja007545

Wing, S., Gkioulidou, M., Johnson, J. R., Newell, P. T., & Wang, C. -P. (2013). Auroral particle precipitation characterized by the substorm cycle. Journal of Geophysical Research: Space Physics, 118, 1022–1039. https://doi.org/10.1002/jgra.50160